ingegneria sismica
International Journal of Earthquake Engineering
Anno XLII – Num.1 - 2025

NUMERICAL SIMULATION STUDY ON THE INFLUENCE OF SEISMIC WAVE PROPAGATION PATHS ON STRUCTURAL VIBRATIONS

Ivan Banović
[1]University of Alaska

SUMMARY: *Seismic waves are influenced by factors such as the path medium and terrain during propagation, leading to changes in waveform, amplitude, and spectral characteristics, which significantly alter the dynamic response of structures. This paper combines the finite element method with ANSYS software to establish a three-dimensional refined model of masonry structures and numerically simulates the effects of seismic waves on masonry buildings. The study concludes that masonry buildings exhibit specific dynamic response patterns under explosive dynamic loads: when conducting seismic safety research on building structures, it is essential to not only reinforce horizontal seismic resistance but also address vertical structural vibration issues. The analytical results obtained using the proposed method are highly accurate, enhancing the precision of seismic dynamic characteristic studies for masonry structures and providing theoretical support for seismic design.*

KEYWORDS: seismic waves, finite element method, structural dynamic response, numerical simulation

1 Introduction

Earthquakes are among the most destructive natural disasters caused by geological activity. They not only result in casualties and property damage but also have significant impacts on surface structures [1, 2]. The propagation of seismic waves is one of the key factors influencing surface structures following an earthquake [3].

Earthquake waves are vibrational waves formed by the energy released from an earthquake source as it propagates through the Earth's interior [4]. Depending on the propagation medium, earthquake waves can be classified into three types: P-waves, S-waves, and surface waves [5]. P-waves are the fastest-propagating waves, capable of traveling through solid, liquid, and gaseous media, with propagation speeds exceeding those at which earthquake waves are generated [6, 7]. S-waves can only propagate through solid media and have slightly lower propagation speeds than P-waves [8]. Surface waves propagate along the ground surface and are influenced only by the surface medium of the Earth's crust, with slower propagation speeds but larger amplitudes [9]. The propagation of seismic waves involves energy transmission through the vibration of the medium, which is influenced by factors such as the medium's elastic parameters and the wave's direction [10, 11].

*i.banovic@gmail.com

The propagation paths of seismic waves include direct paths, reflected paths, and refracted paths, among others. Their impact on surface structures primarily manifests in two aspects: surface vibration and deformation [12, 13]. Surface vibration refers to the ground wave phenomenon centered on the epicenter, caused by seismic waves propagating to the surface [14]. The amplitude, frequency, and duration of vibrations depend on the characteristics of the seismic waves themselves and the surface structure [15]. Intense surface vibrations can cause buildings, bridges, and other structures to resonate, leading to structural damage and collapse [16, 17]. Surface deformation refers to the deformation of the Earth's crust caused by the propagation of seismic waves, including surface subsidence, uplift, cracks, and seismic surface fractures [18, 20]. These deformations can affect land stability and groundwater flow, posing potential hazards to surface structures and the environment [21, 22].

This study first introduces the propagation path of seismic waves in underground rock layers, energy dissipation during transmission, and energy loss when propagating through different media. A new masonry structure finite element model is then established, and ANSYS software is used to perform transient dynamic analysis of structural responses caused by blast vibrations. Finally, numerical simulation methods are employed to study the dynamic response of masonry structures under the influence of explosive seismic waves. The natural frequency is measured using a 941B ultra-low-frequency vibration meter, and time-domain and frequency-domain waveforms are obtained to perform modal analysis on the masonry structure.

2 Seismic wave propagation paths and energy attenuation mechanisms when crossing structural planes

2.1 Seismic wave propagation path

Earthquakes are intense vibrations that propagate through a medium. In underground rock layers, uniformly isotropic media are rarely encountered. Seismic waves travel at different speeds in different media, and their propagation paths are determined by the distribution of their propagation speeds underground. According to Fermat's principle, wave propagation always follows the principle of the path of least time [23]. Therefore, seismic waves only have the shortest spatial distance as their shortest time distance when propagating through a uniform medium. In non-uniform media, the distribution of propagation speeds means that the shortest spatial distance is not the shortest time path. A comparison of the propagation paths of constant wave speeds and linearly increasing wave speeds in the same medium is shown in Figure 1, where (a) and (b) represent the propagation paths under uniform and non-uniform medium conditions, respectively. It can be seen that due to constant changes in speed, the shortest time path of seismic waves in the propagation direction also undergoes constant changes.

Assume that when seismic waves propagate through a medium at a linearly increasing wave velocity, i.e., the wave velocity of the seismic waves is $v(x)$, the hypocenter depth of the earthquake is z, and the horizontal straight-line distance from the hypocenter to the site is x. The propagation distance in the non-uniform medium is shown in Figure 2.

The actual distance of the propagation path can be obtained through the following calculation.

Consider a small seismic wave propagation path element dx and approximate it as a straight line. According to Snell's law, the following relationships hold:

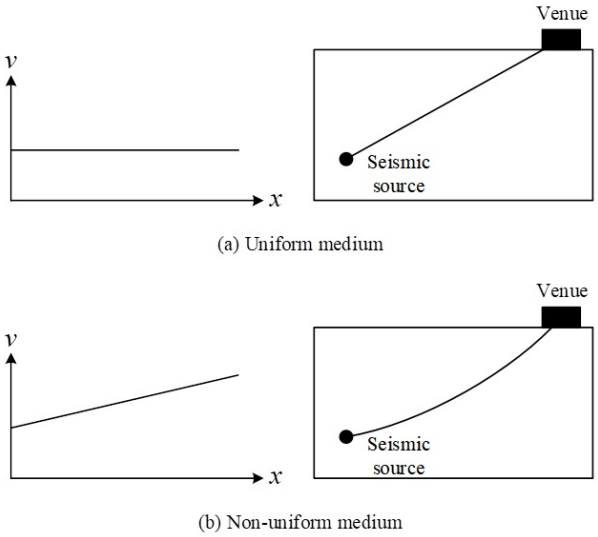

Figure 1: Comparison of propagation paths in uniform and non-uniform media

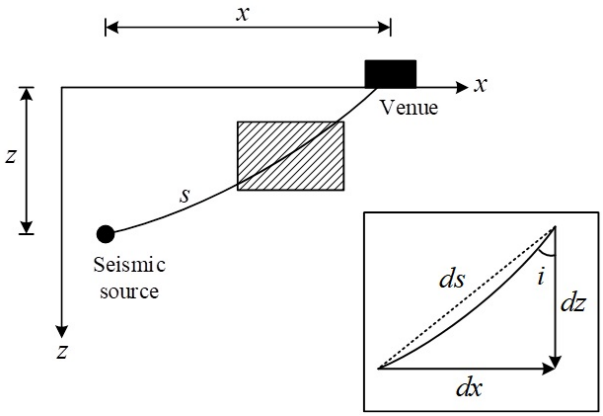

Figure 2: Propagation distance in non-uniform media

$$\begin{cases} \sin i = vp = \dfrac{dx}{ds}, \\ \cos i = \dfrac{dz}{ds} = \sqrt{1-\sin^2 i} = \sqrt{1-v^2p^2}, \\ dx = ds \cdot \sin i = \dfrac{dz}{\cos i}\, vp = \dfrac{vp}{\sqrt{1-v^2p^2}}\, dz, \\ ds = \dfrac{dx}{\sin i} = \dfrac{1}{\sqrt{1-v^2p^2}}\, dz. \end{cases} \tag{1}$$

By integrating Eq. (1), the actual transmission path length s of the seismic wave is obtained as:

$$s = \int_0^z \frac{1}{\sqrt{1-v^2p^2}}\, dz. \tag{2}$$

Similarly, the travel time T of seismic waves from the epicenter to the site is given by:

$$dT = \frac{ds}{v} \quad \Rightarrow \quad T = \int_0^z \frac{1}{v\sqrt{1-v^2p^2}}\,dz. \tag{3}$$

Here, v denotes the seismic wave propagation velocity, p is the ray parameter, i is the incident angle, s is the actual propagation distance, and T is the actual propagation time.

From Eqs. (2) and (3), it is evident that the actual propagation path and travel time of seismic waves are closely related to the source depth, horizontal distance, and the velocity distribution of seismic waves within the medium.

2.2 Dissipation of seismic wave energy

Seismic waves, as a form of vibrational wave, can propagate both through underground media and through the atmosphere. Since air can only be compressed but not sheared, only P-waves can propagate through air, whereas S-waves cannot.

When seismic waves propagate through underground media, their energy gradually attenuates due to the non-uniformity of the medium. This attenuation is influenced by factors such as saturation, frequency, temperature, porosity, pressure, strain amplitude, rock properties, and propagation distance [24].

According to structural dynamics, the amplitude of a particle in a medium as a function of time can be expressed as:

$$x(t) = \bar{x}e^{-\delta t}\cos(\omega t + \varphi_0), \tag{4}$$

where $\bar{x}$ is the initial amplitude of the particle, δ is the decay coefficient ($\delta = v \cdot \omega$, where ω is the angular frequency and v is the damping ratio), and φ_0 is the phase angle.

If the medium is assumed to be completely uniform, isotropic, and elastic, then the amplitude of a particle after time t is equivalent to the amplitude of another particle separated by a time interval t along the propagation path. Hence, the amplitude at any point along the seismic wave propagation direction in such a medium can be written as:

$$x(t) = \bar{x}e^{-\delta\frac{s}{v}}\cos\left(\omega\frac{s}{v} + \varphi_0\right), \tag{5}$$

where s is the distance from the epicenter and v is the seismic wave velocity.

From the relationship between energy and amplitude, the seismic wave energy is given by:

$$E = \tfrac{1}{2}kx^2. \tag{6}$$

Thus, the magnitude of seismic wave energy at a distance s from the source in a homogeneous medium can be determined.

When seismic waves propagate through layered media with different propagation velocities, additional changes in energy occur due to reflection, transmission, and wave type conversion. The energy distribution of seismic waves across such boundaries is typically represented by reflection coefficients (R) and transmission coefficients (T). These coefficients are defined as the ratios of the amplitude (or energy) of reflected and transmitted waves to that of the incident wave, and their values depend on medium density and wave velocity.

To describe this behavior, the concept of wave impedance is introduced. The wave impedance of rock is the product of the P-wave velocity in the rock and its density, representing the power required to produce a unit velocity of moving rock particles when stress waves propagate

through the rock mass. It reflects the rock's resistance to momentum transfer and is expressed as:

$$I = \rho v, \tag{7}$$

where I is the wave impedance, ρ is the medium density, and v is the seismic wave velocity.

The reflection and transmission coefficients are not only related to seismic wave velocity and medium density, but are also affected by the incident angle. Assuming that the seismic wave is vertically incident, the reflection coefficient and transmission coefficient can be derived by solving the Zoeppritz equation, expressed as:

$$R = \frac{\rho_2 v_{p_2} - \rho_1 v_{p_1}}{\rho_1 v_{p_1} + \rho_2 v_{p_2}} = \frac{I_2 - I_1}{I_1 + I_2}, \tag{8}$$

$$T = \frac{2\rho_1 v_{p_1}}{\rho_1 v_{p_1} + \rho_2 v_{p_2}} = \frac{2I_1}{I_1 + I_2}, \tag{9}$$

where R and T denote the reflection and transmission coefficients, respectively, and I_1 and I_2 represent the wave impedances of Medium 1 and Medium 2.

When seismic waves propagate at an oblique angle of incidence, the magnitudes of the reflection and transmission coefficients also vary with the angle. Additionally, because the physical properties of the media above and below the interface differ, seismic waves undergo splitting and mode conversion, resulting in reflected waves P_1 and P_{S_1}, as well as transmitted waves P_2 and P_{S_2}. This process of reflection and transmission is illustrated in Figure 3. In this case, the velocity and density of Medium 1 are greater than those of Medium 2, i.e., $I_1 > I_2$.

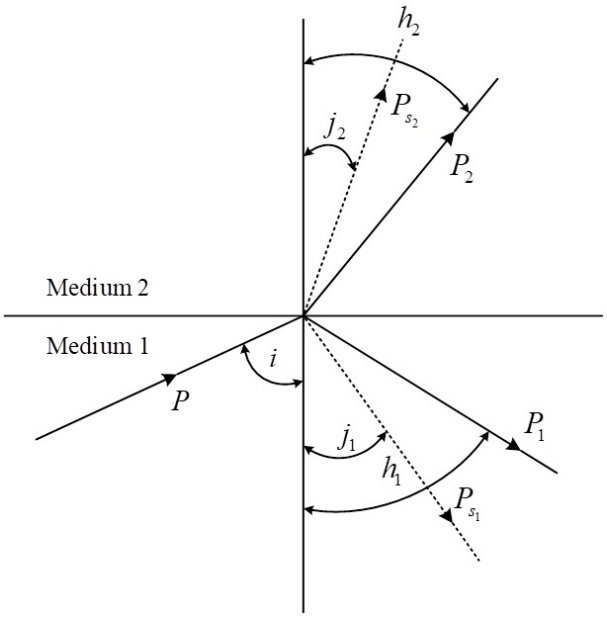

Figure 3: Reflection and transmission of seismic waves

When seismic waves encounter a layered interface, part of the energy is transmitted into the next medium with the transmitted waves, while part of the energy is retained in the original medium due to reflection.

The ratio of retained energy to the total incident energy is called the energy retention ratio w, which can be calculated as:

$$w = 1 - R_p^2 - \alpha_{s_2} R_s^2 - (1 - s)\left(\alpha_p^2 T_p^4 + \alpha_{s_1}^2 T_s^4\right), \tag{10}$$

where $\alpha_p = \frac{\rho_1 v_{p_1}}{\rho_2 v_{p_2}}$, $\alpha_{s_1} = \frac{\rho_1 v_{s_1}}{\rho_2 v_{p_2}}$ and $\alpha_{s_2} = \frac{\rho_2 v_{s_2}}{\rho_2 v_{p_2}}$.

Here, R_p and R_s are the P-wave and SV-wave reflection coefficients, T_p and T_s are the P-wave and SV-wave transmission coefficients, respectively, and s denotes the energy attenuation ratio, i.e., the proportion of energy attenuated when the transmitted wave propagates through Medium 1 to the free surface, reflects back, and re-enters the medium interface, relative to the initial transmitted energy at the interface.

3 Finite element dynamic analysis

The finite element method (FEM) is a widely used computational approach in engineering for solving complex structural and physical problems. The basic idea of FEM is to divide the solution domain into a finite number of small elements connected at nodes. Equations are then formulated for these nodes based on equilibrium or energy relationships, and the individual element equations are assembled to form a global system of algebraic equations. After boundary conditions are applied, this system can be solved numerically to obtain the desired response. FEM is highly effective in modern engineering practice due to its implementation in computer programs.

Among the many general-purpose and specialized finite element software packages, ANSYS is one of the most widely used commercial tools. ANSYS is a large-scale, general-purpose computer-aided engineering (CAE) software based on FEM. It is extensively applied across diverse industries, including mechanical manufacturing, petrochemicals, shipbuilding, aerospace, automotive, electronics, civil engineering, water resources, railways, household appliances, biology, and medicine. It provides capabilities for structural, thermal, fluid, electromagnetic, and acoustic analyses, and can address steady-state, transient, linear, and nonlinear problems, including stress, heat conduction, fluid flow, and electromagnetic field analysis [25].

ANSYS software is composed of three main components: the preprocessing module, the analysis and calculation module, and the postprocessing module. The preprocessing module provides solid modeling and mesh generation tools that allow users to construct finite element models easily. The software supports over 100 element types, enabling the simulation of a wide range of engineering materials and structures. The analysis and computation module includes linear, nonlinear, and highly nonlinear structural analysis; fluid dynamics; electromagnetic field analysis; acoustic field analysis; piezoelectric analysis; and multiphysics coupled analysis. It also supports sensitivity and optimization analyses, as well as the simulation of interactions between multiple physical domains. Finally, the postprocessing module allows visualization of results through contour plots, gradient plots, vector plots, trajectory plots, 3D slices, and semi-transparent views. Results can also be exported in chart or curve formats, facilitating detailed interpretation of structural behavior.

3.1 Theoretical basis of the finite element method

Solving mechanical problems using the finite element method generally involves two main stages. First, an element characteristic analysis is carried out to establish the element-level stiffness equations (equilibrium equations), leading to the element stiffness matrix:

$$[K]^e\{\delta\}^e = \{R\}^e. \tag{11}$$

Next, a comprehensive structural analysis is performed by combining the stiffness equations

of all elements to obtain the total stiffness equation of the structure:

$$[K] = \sum [K]^e = \sum A^T K^e A. \tag{12}$$

The fundamental formula system used in these calculations includes several key relations. The element stiffness calculation is given by

$$[K]^e = \int_{V_e} [B]^T [D][B]\, dv, \tag{13}$$

where $[B]$ is the geometry matrix determined by the element shape functions and node displacements, and $[D]$ is the elasticity matrix, dependent on the material properties E and v.

The assembly of element stiffness matrices follows

$$[K] = \sum A^T K A, \tag{14}$$

while the nodal load for an element is calculated by

$$\{p\}^e = \int [N]^T \{p\}\, ds. \tag{15}$$

The assembly of nodal loads is expressed as

$$(P) = AP^e, \tag{16}$$

and the displacement constraint relationship is

$$\{d\} = \{\bar{d}\}. \tag{17}$$

The global stiffness equation is therefore

$$[K]\{\delta\} = \{P\} \quad \Rightarrow \quad \{\delta\} = [K]^{-1}\{P\}. \tag{18}$$

Once the displacements are determined, strains are calculated as

$$\{\varepsilon\} = [B]\{\delta\}, \tag{19}$$

and stresses are determined by

$$\{\sigma\} = [D][B]\{\delta\}. \tag{20}$$

Finally, the support reaction forces are obtained through

$$R_i = K_{ii}\overline{d_i}. \tag{21}$$

3.2 Computing Unit

This paper adopts a four-node plane isoparametric element, referred to in ANSYS as the PLANE42 element. By setting the appropriate element options, PLANE42 can be applied for either plane stress analysis or plane strain analysis. Each element has four nodes, with two degrees of freedom at each node in the X and Y directions. The PLANE42 element includes properties such as plasticity, creep, shear expansion, stress hardening, and large deformation.

The shape functions of the PLANE42 element are defined as:

$$\begin{cases} N_1 = \frac{1}{4}(1-\xi)(1-\eta), \\ N_2 = \frac{1}{4}(1+\xi)(1-\eta), \\ N_3 = \frac{1}{4}(1+\xi)(1+\eta), \\ N_4 = \frac{1}{4}(1-\xi)(1+\eta). \end{cases} \tag{22}$$

In general form:

$$N_i(\xi,\eta) = \tfrac{1}{4}(1+\xi_i\xi)(1+\eta_i\eta), \quad i = 1,2,3,4. \tag{23}$$

The coordinates of any point within the element, (x,y), are related to the nodal coordinates through the shape functions:

$$\begin{cases} x(\xi,\eta) = \sum_{i=1}^{4} N_i x_i = N_1x_1 + N_2x_2 + N_3x_3 + N_4x_4, \\ y(\xi,\eta) = \sum_{i=1}^{4} N_i y_i = N_1y_1 + N_2y_2 + N_3y_3 + N_4y_4. \end{cases} \tag{24}$$

Similarly, the field variables u,v at any point within the element are related to the nodal values through the shape functions:

$$\begin{cases} u(\xi,\eta) = N_1u_1 + N_2u_2 + N_3u_3 + N_4u_4, \\ v(\xi,\eta) = N_1v_1 + N_2v_2 + N_3v_3 + N_4v_4. \end{cases} \tag{25}$$

Using the same shape functions N to represent both the geometric form of the element and the distribution of field variables defines the element as isoparametric. Based on these properties, the shape functions map nodes in the local coordinates (ξ,η) of a standard square to the corresponding nodes in any quadrilateral of the global coordinate system. Thus, the coordinate transformation relationship is expressed as:

$$x = \sum_{i=1}^{4} N_i x_i, \qquad y = \sum_{i=1}^{4} N_i y_i. \tag{26}$$

In matrix form, this can be written as:

$$\begin{bmatrix} x \\ y \end{bmatrix} = \begin{bmatrix} N_1 & 0 & N_2 & 0 & N_3 & 0 & N_4 & 0 \\ 0 & N_1 & 0 & N_2 & 0 & N_3 & 0 & N_4 \end{bmatrix} \begin{bmatrix} x_1 \\ y_1 \\ x_2 \\ y_2 \\ x_3 \\ y_3 \\ x_4 \\ y_4 \end{bmatrix}. \tag{27}$$

Similarly, after the above transformation, the displacement function can be written as:

$$\{u\} = \begin{bmatrix} u \\ v \end{bmatrix}_{(x,y)} = \begin{bmatrix} N_1 & 0 & N_2 & 0 & N_3 & 0 & N_4 & 0 \\ 0 & N_1 & 0 & N_2 & 0 & N_3 & 0 & N_4 \end{bmatrix}_{(\xi,\eta)} \begin{bmatrix} u_1 \\ v_1 \\ u_2 \\ v_2 \\ u_3 \\ v_3 \\ u_4 \\ v_4 \end{bmatrix}. \tag{28}$$

Here, $N_i(\xi,\eta)$ is a function of ξ,η, not of x,y.

The strain–displacement relationship, according to elasticity theory, links strain $\{\varepsilon\}$ and nodal displacement $\{\delta\}^e$ in a plane problem as:

$$\{\varepsilon\} = \begin{bmatrix} \frac{\partial}{\partial x} & 0 \\ 0 & \frac{\partial}{\partial y} \\ \frac{\partial}{\partial y} & \frac{\partial}{\partial x} \end{bmatrix} \{u\} = \begin{bmatrix} \frac{\partial}{\partial x} & 0 \\ 0 & \frac{\partial}{\partial y} \\ \frac{\partial}{\partial y} & \frac{\partial}{\partial x} \end{bmatrix} [N]\{\delta\}^e = [B]\{\delta\}^e. \tag{29}$$

The geometric matrix $[B]$ is given by:

$$[B] = \begin{bmatrix} \frac{\partial N_1}{\partial x} & 0 & \frac{\partial N_2}{\partial x} & 0 & \frac{\partial N_3}{\partial x} & 0 & \frac{\partial N_4}{\partial x} & 0 \\ 0 & \frac{\partial N_1}{\partial y} & 0 & \frac{\partial N_2}{\partial y} & 0 & \frac{\partial N_3}{\partial y} & 0 & \frac{\partial N_4}{\partial y} \\ \frac{\partial N_1}{\partial y} & \frac{\partial N_1}{\partial x} & \frac{\partial N_2}{\partial y} & \frac{\partial N_2}{\partial x} & \frac{\partial N_3}{\partial y} & \frac{\partial N_3}{\partial x} & \frac{\partial N_4}{\partial y} & \frac{\partial N_4}{\partial x} \end{bmatrix}. \tag{30}$$

Assuming the soil is a homogeneous, isotropic, and elastic body, the stress–strain relationship is expressed as:

$$\{\sigma\} = [D]\{\varepsilon\} = [D][B]\{\delta\}^e. \tag{31}$$

The elasticity matrix $[D]$ is:

$$[D] = \begin{bmatrix} E & F & 0 \\ F & E & 0 \\ 0 & 0 & G \end{bmatrix}, \tag{32}$$

where, for plane strain problems:

$$E = \frac{E(1-\mu)}{(1+\mu)(1-2\mu)}, \quad F = \frac{\mu E}{(1+\mu)(1-2\mu)}, \quad G = \frac{E}{2(1+\mu)}. \tag{33}$$

Finally, the element stiffness matrix of PLANE42 is obtained as:

$$[K]^* = \iint_{\Omega} [B]^T [D][B]\, dx\, dy. \tag{34}$$

3.3 Structural dynamics analysis

Based on the type of dynamic loads acting on a structure, structural dynamics analysis can be categorized into several major types: modal analysis, transient dynamics analysis, harmonic response analysis, and spectral analysis. Simple harmonic loads correspond to harmonic response analysis, random loads correspond to spectral analysis, and impact loads, sudden loads, and rapidly moving loads correspond to transient dynamics analysis.

The ultimate goal of structural dynamic analysis is to determine the time-dependent variation of internal forces, displacements, and other response parameters under dynamic loads, thereby identifying their maximum values as a basis for design or verification.

Since the primary objective of this study is to investigate the influence of seismic wave propagation paths on structural vibrations, the transient dynamic analysis method is adopted for time-history analysis, referencing seismic load calculation methods.

Transient dynamic analysis calculates the response of a structure under loads that vary arbitrarily over time, also referred to as time-history analysis. This method can be used to determine the time-dependent variation of displacement, stress, and strain in structures subjected to static, transient, or harmonic loads. A key characteristic of transient analysis is the necessity to account for the effects of inertial forces and damping. If these effects are negligible, static analysis may be used as an alternative to transient dynamic analysis. The governing equation is expressed as:

$$[M]\{\ddot{u}\} + [C]\{\dot{u}\} + [K]\{u\} = \{F(t)\}, \tag{35}$$

where $[M]$ is the mass matrix, $[C]$ is the damping matrix, $[K]$ is the stiffness matrix, $\{u\}$ is the nodal displacement vector, $\{\dot{u}\}$ is the nodal velocity vector, and $\{\ddot{u}\}$ is the nodal acceleration vector.

For any given time t, the transient dynamics equations can be regarded as static equilibrium equations with added inertial and damping forces. ANSYS employs a time-integration method to solve this system of equations on a discrete time and spatial grid.

4 Numerical simulation analysis of buildings under seismic waves

The study selected a newly developed residential community in City H as the research object. The floor plan of the masonry building is shown in Figure 4.

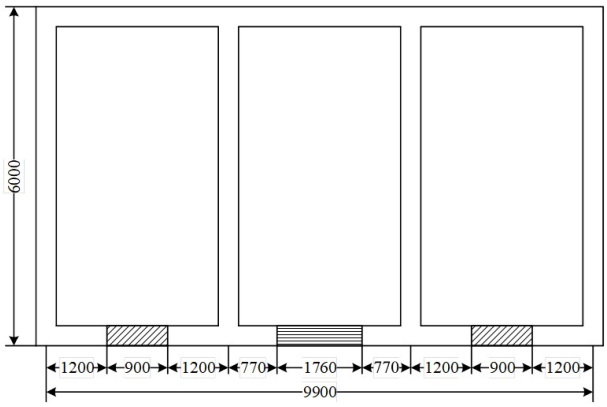

Figure 4: Part plan view of the masonry building structure

4.1 Numerical calculation model

To make the model's response more closely resemble the actual structure, a two-dimensional finite element model is used for the computational analysis. To reduce computational complexity, several basic assumptions are made. Masonry is considered an isotropic material. Due

to the significant variations in the mechanical properties of masonry, it can be regarded as a two-phase material, consisting of elastic blocks (such as bricks or concrete blocks) embedded in a non-elastic mortar matrix. Although two-phase heterogeneous finite element models have been adopted by some scholars, such models complicate the analysis. Therefore, to simplify the problem, the model assumes that masonry is a single-phase homogeneous and isotropic material. Additionally, the floor slab is assumed to have infinite stiffness within its own plane.

The masonry building has a span of 3.5 m, a depth of 6 m, and a height of 2.8 m. The window length is 1.25 m with a width of 1 m, and the window sill is located 1.2 m above the ground. The door width is 1.8 m. The material properties of the masonry are shown in Table 1.

Table 1: Parameters of the material properties of masonry

Unit	Material grade	Density (Kg/m^3)	Tensile strength (MPa)	Compressive strength (MPa)	Elastic modulus (GPa)	Poisson's ratio
Masonry	Plain block	2000	0.16	20	40	0.16

Based on the ANSYS input parameters listed in Table 1, the front view and rear view of the finite element model constructed are shown in Figures 5 and 6, respectively.

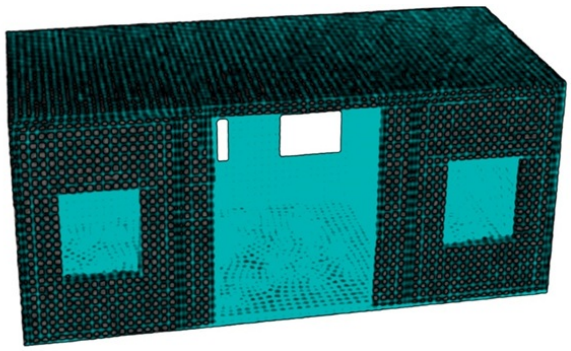

Figure 5: Front view of the finite element model

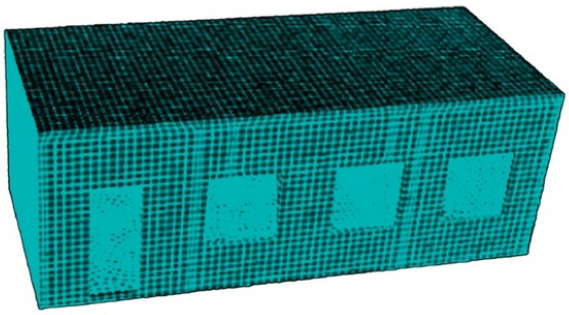

Figure 6: Rear view of the finite element model

4.2 Testing the vibration characteristics of masonry structures

This study employed the 941B-type ultra-low-frequency vibration meter developed by the Institute of Engineering Mechanics of the China Earthquake Administration. An external amplifier and specialized coherent time-domain and frequency-domain data processing software were used to conduct dynamic characteristic tests. The vibration sensor was positioned as close as

possible to the stiffness center of the building's planar location. During installation, the sensor was adjusted to capture only translational signals to avoid altering vibration records. The structural vibration power spectrum was obtained by analyzing the time-domain data from the vibration tests. A low-pass filter was applied during data analysis to eliminate noise interference regions in the vibration waveforms, from which frequencies were extracted, yielding both time-domain and frequency-domain waveforms.

The three-component vibration data measured at the test points are presented in Figures 7–9, where subfigures (a) and (b) represent the time-history diagram and frequency-domain diagram, respectively. The time-history diagrams reveal that among the vibration curves in different directions, the vertical (Z-direction) vibration velocity is the largest, followed by the horizontal (X-direction), while the longitudinal (Y-direction) vibration velocity is the smallest. This indicates that when conducting seismic safety assessments of building structures under blast-induced seismic waves, it is necessary not only to reinforce horizontal seismic resistance but also to address vibration issues in the vertical direction. The frequency-domain diagrams show that 3.1 Hz, 5.1 Hz, and 7.6 Hz represent the low-order natural frequencies of the building.

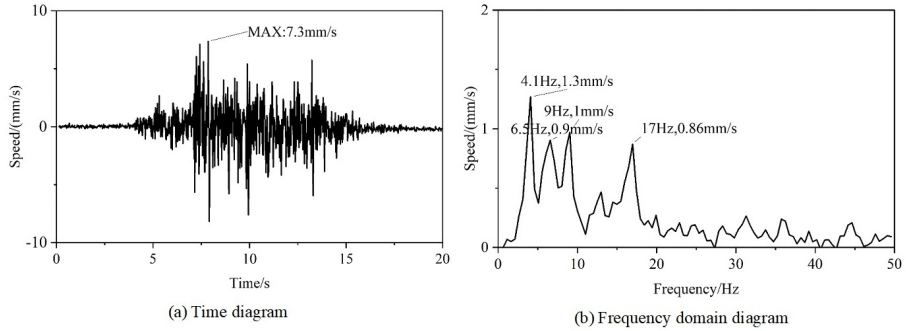

Figure 7: Vibration characteristics in the X-direction

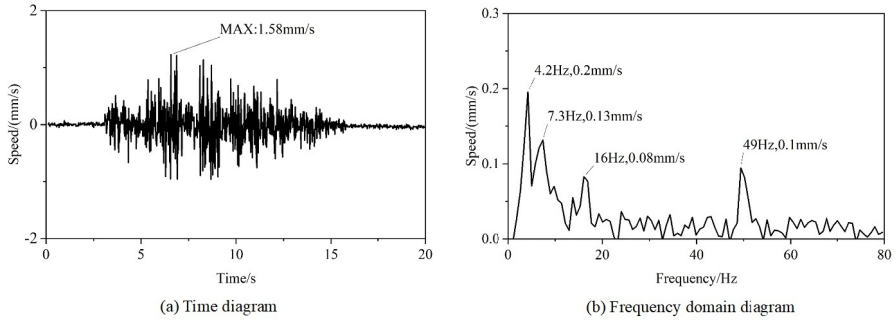

Figure 8: Vibration characteristics in the Y-direction

4.3 Modal analysis results

The low-order mode shapes obtained from the modal analysis are illustrated in Figures 10 to 12. The first and second mode shapes of the structure correspond to translational motions, while the third mode shape represents a torsional motion.

A comparison between the measured and simulated low-order natural frequencies and periods is provided in Table 2. The finite element analysis results for the first three frequencies

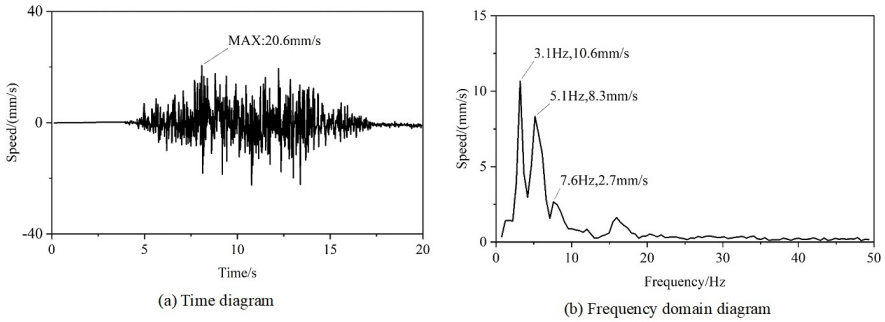

Figure 9: Vibration characteristics in the Z-direction

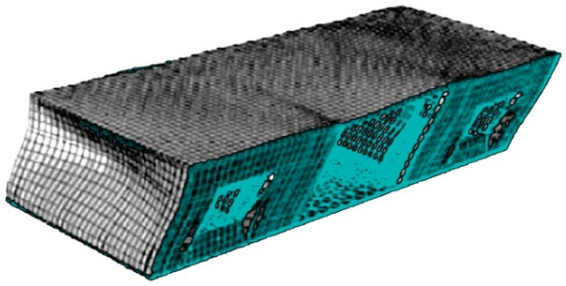

Figure 10: First mode: longitudinal translation

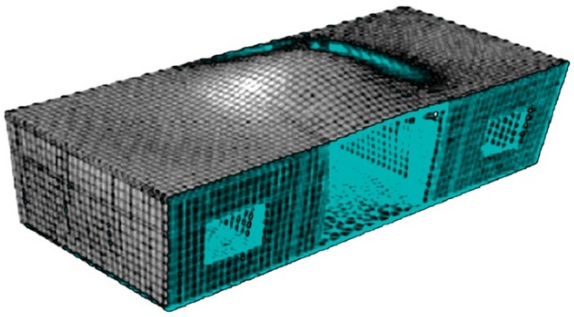

Figure 11: Second mode: vertical vibration

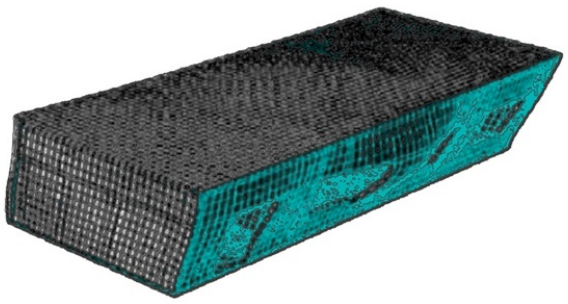

Figure 12: Third mode: transverse translation

and periods show good agreement with the experimental measurements, indicating the high reliability and accuracy of the simulation results.

Table 2: Comparison of measured and simulated natural frequencies and periods

Mode	Frequency (Hz)		Period (s)	
	Measured	Simulated	Measured	Simulated
1	4.1	4.3	0.22	0.23
2	5.2	5.5	0.22	0.20
3	7.3	7.5	0.15	0.16

4.4 Comparison of schedule analysis results and actual measurement data

The acceleration time history, derived from the ground-measured velocity time history, is used as the input excitation for structural vibration analysis. The structural response is then calculated and compared with the simulation results. Simultaneous triaxial blast seismic waves are applied to obtain the acceleration time history curve. The measured velocity time history curves of the top floor slab of the masonry structure in the X- and Z-directions were converted into acceleration time history curves and compared with the acceleration time history curves obtained from finite element simulations, as shown in Figure 13. Subfigures (a) and (b) represent the X- and Z-direction acceleration time history curves, respectively.

From this comparison, it can be observed that the measured acceleration response of the masonry building structure is greater than the simulated response, but the difference between the two is not significant. This discrepancy may be due to simplifications in the model: the bottom of the model is constrained as a fixed support, whereas the foundation of the actual structure does not behave as an ideal fixed constraint. Ignoring the vibration of the floor also introduces inevitable discrepancies. Additionally, the simulated X-direction acceleration time history lags behind the measured response, likely because of insufficient stiffness in the model, which causes the simulated acceleration response to evolve more slowly.

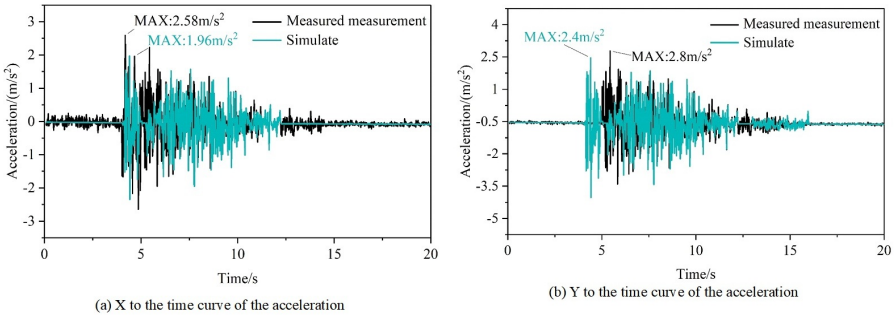

Figure 13: Comparison between measured and simulated acceleration curves

5 Conclusion

This paper employs ANSYS software to investigate the impact of seismic wave propagation paths on structural vibrations, leading to the following conclusions.

The time history diagrams show that the vertical (Z-direction) vibration velocity is the largest, followed by the horizontal (X-direction), while the longitudinal (Y-direction) vibration velocity is the smallest. Therefore, when conducting seismic safety research on building structures under the influence of blast seismic waves, it is necessary not only to strengthen seismic design in the horizontal directions but also to address vibration issues in the vertical direction.

The finite element analysis results for the first three natural frequencies and periods are generally consistent with the measured results, demonstrating the high reliability of the finite element simulation.

The measured acceleration response is greater than the simulated acceleration response, but the difference between the two remains small, further confirming the reliability and accuracy of the finite element simulation results.

References

[1] Bojadjieva, J., Sheshov, V., & Bonnard, C. (2018). Hazard and risk assessment of earthquake-induced landslides—case study. *Landslides, 15*(1), 161-171.

[2] Daniell, J. E., Schaefer, A. M., & Wenzel, F. (2017). Losses associated with secondary effects in earthquakes. *Frontiers in Built Environment, 3*, 30.

[3] Hanyga, A. (Ed.). (2016). *Seismic Wave Propagation in the Earth*. Elsevier.

[4] Golubev, V., Shevchenko, A., & Petrov, I. (2020). Simulation of seismic wave propagation in a multicomponent oil deposit model. *International Journal of Applied Mechanics, 12*(08), 2050084.

[5] Mohamed, T., Duriez, J., Veylon, G., Peyras, L., & Soulat, P. (2023). A discrete-based multi-scale modeling approach for the propagation of seismic waves in soils. *Soil Dynamics and Earthquake Engineering, 173*, 108104.

[6] Zong, Z., Yin, X., & Wu, G. (2015). Complex seismic amplitude inversion for P-wave and S-wave quality factors. *Geophysical Journal International, 202*(1), 564-577.

[7] Dumke, I., & Berndt, C. (2019). Prediction of seismic P-wave velocity using machine learning. *Solid Earth, 10*(6), 1989-2000.

[8] Stucchi, E., Tognarelli, A., & Ribolini, A. (2017). SH-wave seismic reflection at a landslide (Patigno, NW Italy) integrated with P-wave. *Journal of Applied Geophysics, 146*, 188-197.

[9] Levshin, A. L., Barmin, M. P., & Ritzwoller, M. H. (2018). Tutorial review of seismic surface waves' phenomenology. *Journal of Seismology, 22*(2), 519-537.

[10] Ma, J., Yang, D., Tong, P., & Ma, X. (2018). TSOS and TSOS-FK hybrid methods for modelling the propagation of seismic waves. *Geophysical Journal International, 214*(3), 1665-1682.

[11] Pavlenko, O., & Kozlovskaya, E. (2018). Characteristics of radiation and propagation of seismic waves in Northern Finland, estimated based on records of local earthquakes. *Pure and Applied Geophysics, 175*(12), 4197-4223.

[12] He, S., Chen, T., Vennes, I., He, X., Song, D., Chen, J., & Mitri, H. (2020). Dynamic modelling of seismic wave propagation due to a remote seismic source: A case study. *Rock Mechanics and Rock Engineering, 53*, 5177–5201.

[13] Margerin, L. (2021). Seismic waves, scattering. In *Encyclopedia of Solid Earth Geophysics* (pp. 1537-1550). Cham: Springer International Publishing.

[14] Filipiak, J., & Marć, P. (2021). Surface acoustic wave vibration sensor as a seismometer. *Sensors and Actuators A: Physical, 323*, 112653.

[15] Dudchenko, A. V., Dias, D., & Kuznetsov, S. V. (2021). Vertical wave barriers for vibration reduction. *Archive of Applied Mechanics, 91*(1), 257-276.

[16] Li, J. C., Li, N. N., Chai, S. B., & Li, H. B. (2018). Analytical study of ground motion caused by seismic wave propagation across faulted rock masses. *International Journal for Numerical and Analytical Methods in Geomechanics, 42*(1), 95-109.

[17] Berngardt, O. I., Perevalova, N. P., Podlesnyi, A. V., Kurkin, V. I., & Zherebtsov, G. A. (2017). Vertical midscale ionospheric disturbances caused by surface seismic waves based on Irkutsk chirp ionosonde data in 2011–2016. *Journal of Geophysical Research: Space Physics, 122*(4), 4736-4754.

[18] Kuzmin, Y. O. (2020). Recent geodynamics and slow deformation waves. *Izvestiya, Physics of the Solid Earth, 56*(4), 595-603.

[19] Stähler, S. C., Panning, M. P., Vance, S. D., Lorenz, R. D., van Driel, M., Nissen-Meyer, T., & Kedar, S. (2018). Seismic wave propagation in icy ocean worlds. *Journal of Geophysical Research: Planets, 123*(1), 206-232.

[20] Apostol, B. F. (2022). Near-Field Seismic Motion: Waves, Deformations and Seismic Moment. *Axioms, 11*(8), 409.

[21] Birger, B. I. (2020). Recent movements of the earth's surface and stress propagation in the elastic upper crust. *Izvestiya, Physics of the Solid Earth, 56*(4), 585-594.

[22] Ali, M., Shahzad, M. I., Nazeer, M., Mahmood, I., & Zia, I. (2021). Estimation of surface deformation due to Pasni earthquake using RADAR interferometry. *Geocarto International, 36*(14), 1630-1645.

[23] Fontara, I. K., Schepers, W., Savidis, S., & Rackwitza, F. (2017). FE/PML numerical schemes for dynamic soil-structure interaction and seismic wave propagation analysis. *Procedia Engineering, 199*, 2348-2353.

[24] Qian, Z., Zhang, D., Liao, H., & Wang, H. (2024). Can the seismic wave attenuation characteristics of various soils be identified using distributed acoustic sensing?. *Journal of Applied Geophysics, 221*, 105281.

[25] Kaya, K., Dorduncu, M., & Madenci, E. (2025). Variable horizon ordinary state-based peridynamic analysis in ANSYS framework. *Mechanics of Advanced Materials and Structures, 32*(9), 2079-2095.